Weighted Energy Efficiency Maximization for a UAV-Assisted Multi-Platoon Mobile Edge Computing System

Xuting Duan, Yukang Zhou, Daxin Tian, *Senior Member, IEEE*, Jianshan Zhou, Zhengguo Sheng, *Senior Member, IEEE*, Xuemin (Sherman) Shen, *Fellow, IEEE*

***Abstract*—With the rapid development of mobile computing, mobile edge computing has increasingly become an essential means to meet the computing power requirements of intelligent networked vehicles. However, users with high mobility and coupled dynamics are rarely considered in the edge computing paradigms. In this paper, we studied a UAV-assisted mobile edge computing system with multi-platoon vehicles. Our paper aims to maximize the system's weighted global energy efficiency, which can flexibly adjust each vehicle's energy consumption according to user preferences and system needs. In particular, we design a controller for platooning vehicles based on a two-dimensional path-following model and Frenet frames, and model the coupled characteristics of air-to-ground communications and onboard computation. Furthermore, due to the non-convexity of the objective function and constraints of the optimization problem, we propose an optimization algorithm based on the sequential quadratic programming method. The simulation results show that the proposed method significantly surpasses conventional schemes.**

***Index Terms*—Unmanned aerial vehicle, mobile edge computing, energy efficiency, vehicle platooning.**

I. Introduction

A. Background

With the development of V2X communication technologies and the applications of AI-based algorithms, intelligent and networked platooning vehicles are increasingly becoming an essential means to improve road utilization efficiency and alleviate congestion [1]. Therefore, they are considered to be a critical part of the future intelligent autonomous transportation systems. However, vehicle information exchange, which is necessary for stable and efficient control of vehicle platoons, requires the assistance of a high-stability and low-latency network. Furthermore, considering the intelligent autonomous driving assistance of a platoon, there is a contradiction between the requirements of the computation-intensive, delay-sensitive tasks and limited computation resources of vehicles. Applications ranging from advanced driving assistance services such as multi-source heterogeneous data fusion, perception of the surrounding traffic conditions, and driving decision-making to in-car entertainment services like virtual reality video games urgently need assistance from external computing platforms [2]–[4]. Therefore, advanced communication and auxiliary computing technology will greatly promote the realization of intelligent autonomous transport systems.

Currently, existing connected vehicles' communication devices and networking capabilities are insufficient to meet the aforementioned requirements. Fortunately, the vision of Beyond-5G/6G provides us with a spacial wireless network alternative, including terrestrial, air-to-ground (A2G), or spacial networking. When facing specific scenarios, such as disaster relief situations or destroyed area connectivity, the A2G network is an encouraging and reliable means. Mobile edge computing (MEC) is a promising paradigm to provide computing resources [5]–[7], and the users can place it on unmanned aerial vehicles (UAVs) to enhance the implementability [8]–[10]. Thus, UAVs equipped with MEC capability play a role as network infrastructure providers. The UAVs and platooning vehicles can form A2G vehicular network systems to provide computation and communication services to users. Users can offload their computationally-intensive tasks to the MEC servers, which dramatically shortens the calculation time and improves users' quality of experience. Therefore, it is relevant to investigate further the MEC resources' management and the A2G network cooperation.

Although the UAV-to-vehicles communication and computation system is regarded as a practical idea to promote the application of intelligent autonomous transport systems [11], [12], there are some challenges to be settled because of the constrained resources and complex dynamics of two-dimensional platooning vehicles. Specifically, the connected vehicles work as task providers for the flying MEC node and terminal users of A2G cooperative networks in the MEC system, whose high mobility and mutually influenced two-dimensional dynamics are coupled into the communication channel. As a result, the system is more complex and costly to

This research was supported in part by the National Natural Science Foundation of China under Grant No. 62173012, U20A20155, in part by the Beijing Municipal Natural Science Foundation under Grant No. L191001, in part by the Newton Advanced Fellowship under Grant No. 62061130221, in part by State Key Laboratory of Air Traffic Management System and Technology under Grant No. SKLATM202103. (Corresponding author: Xuting Duan)

Xuting Duan, Yukang Zhou, Daxin Tian and Jianshan Zhou are Beijing Advanced Innovation Center for Big Data and Brain Computing, Beijing Key Laboratory for Cooperative Vehicle Infrastructure Systems & Safety Control, the School of Transportation Science and Engineering, Beihang University, Beijing 100191, China (e-mail:duanxuting@buaa.edu.cn, 1027511462@qq.com, dtian@buaa.edu.cn, jianshanzhou@foxmail.com).

Zhengguo Sheng is with the Department of Engineering and Design, the University of Sussex, Richmond 3A09, UK (e-mail: z.sheng@sussex.ac.uk).

Xuemin Shen is with the Electrical and Computer Engineering Department, University of Waterloo, Waterloo, ON N2L 3G1, Canada (e-mail: sshen@uwaterloo.ca).

solve. Another challenge is the limited onboard energy of the UAV, and the operating time of the UAV is severely restricted by the energy it carries. Thus the limited energy needs to be well scheduled by optimizing communication and computation resources to improve the energy efficiency of MEC service to guarantee the quality of service (QoS) of the UAV-enabled MEC system.

B. Related Works and Motivation

Mobile edge computing with the implement of unmanned aerial vehicle networks has been widely investigated from the perspective of resource scheduling and UAV trajectory design [6], [13]–[17]. For example, [14], [15] have studied the scenario that UAVs equipped with MEC servers provide edge computing services to fixed users. Further, the maximization of the system-wide computation rate [14] and communication energy consumption [15] are constructed as objective of the resource allocation problems, respectively, through the joint optimization of the system's communication and computing resources and the trajectory of the UAV. Differently, in [16], Zhang *et al.* have considered mobile users in UAV-assisted MEC systems, which are defined as pedestrians with a predetermined trajectory and low mobility. In [13], Liu *et al.* have further considered one-dimensional connected vehicle platoons, and jointly scheduled transmission power, communication and computation time allocation scheme to maximize computing rate. A modified SQP algorithm is applied to efficiently solve the non-convex problem. The offloading ratio of users' computing tasks and trajectory of the UAV are jointly optimized to maximize a linear function that includes calculation delay and energy consumption in [16]. Besides, users with high mobility like connected vehicles are introduced in UAV-aided vehicular networks in [17]. And the communication resources such as transmission power and time allocation scheme are optimized to the system's overall energy efficiency [17]. However, to face the big wave of intelligent connected vehicles [18], [19], the two-dimensional dynamic characteristics of intelligent vehicle platoons and their impact on G2A communication channels and onboard computing need to be jointly investigated.

The resource scheduling of swarm of intelligent connected vehicles have been extensively studied as a promising approach to improve road safety and traffic efficiency [20]–[24]. In [20], Peng *et al.* jointly optimize the computing resources, spectrum allocation and vehicles' cache amount through a multi-agent deep deterministic policy gradient (MADDPG)-based method, where the number of offloaded tasks is constructed as the system objective. In [21], Mei *et al.* have scheduled the radio resource allocation in LTE-V2V network in order to minimize vehicle platoon's tracking error. In [22], Hegde *et al.* have scheduled 3GPP radio and vehicle mobility management to improve vehicular networks' QoS. Differently, in [24], Hegde *et al.* optimized time and subchannel allocation scheme to improve the QoS of vehicular networks based on sidelink group scheduling and mobility for platoons. In [23], radio resource management is considered to maximize a holistic reward function for the group's collective success based on multi-agent reinforcement learning (MARL) approach. In these representative works [21]–[23], resource scheduling in vehicular networks has been extensively researched to enhance the vehicle platooning strategy's effectiveness and reliability or vehicular network quality, while the computing ability of the vehicle platoon is often assumed to be sufficient. These scenarios are not practical when the vehicles need to handle computation-intensive, delay-sensitive tasks. Thus, mobile edge computing (MEC) needs to be introduced to assist vehicle platoon in computing, and the impact of vehicle mobility on communication and computation resource allocation need to be jointly considered.

Constrained by the limited battery energy and QoS requirements, a performance metric named computation efficiency is defined as the objective of the resource allocation problem of UAV-enabled mobile edge computing systems. The authors in [25] and [26] have defined computation efficiency as the computed data (bit) divided by the energy consumed by the computation process (Joule). In [25], Sun *et al.* have jointly optimized the transmission power, communication time and MEC frequency to maximize computation efficiency with the help of iterative and gradient descent methods. In [26], Zhou *et al* have also aimed at optimizing the energy harvesting time, the local computing frequency, the offloading time, and the power to maximize the computation efficiency. In addition to computation efficiency, energy efficiency is mostly defined as the ratio of offloaded data to the system's energy consumption [27]. In [27], Li *et al.* have maximized the energy efficiency of the UAV and jointly optimized the offloading of the computing task and the UAV trajectory based on the Dinkelbach algorithm and the successive convex approximation (SCA) technique. In [28], Wu *et al.* have proposed a three-layer computation offloading strategy combining the UAV position optimization and the Long Short-Term Memory (LSTM)-based task prediction algorithms to maximize the energy efficiency of the UAV-enabled MEC system. However, existing works [17], [25]–[30] mostly take the direct addition of computed data (bit) and energy consumption as the component of objective function, while it is necessary to consider environmental factors or user preferences in the optimization objective for actual application scenarios.

C. Contributions

It can be seen from the related works mentioned above that few researches have focused on the resource scheduling of UAV-assisted MEC system with vehicles in a two-dimensional multi-lane platoon as end users. And user's preferences in energy consumption is rarely considered in system performance metric. Towards this end, this paper investigates a new UAV-assisted MEC system for multi-platoon mobile users, aiming to maximize a weighted energy efficiency of MEC service as performance metric. Specifically, a UAV acts as an MEC node and multi-platoon vehicles are mobile terminal users in the MEC system, in which the characteristics of vehicle dynamics are integrated into G2A communication channel. In order to reflect user preferences and system requirements on energy consumption in system performance metric, we

adjust the energy component of the system energy efficiency. Communication resources are optimized to maximize it. The main contributions of this paper are summarized as follows:

- We formulate a UAV-enabled MEC network system for multi-platoon vehicles. First, we establish a two-dimensional stable vehicle formation steering model by simulating the driving behavior of human drivers. Then, its effect on G2A communication and task offloading is integrated into the system model. Furthermore, we introduce the Frenet coordinate system to reduce the complexity of vehicle formation control.
- A form of weighted global energy efficiency is formulated as the objective function to combine user preference into system metric. An iterative interior-point-based algorithm is proposed to decompose the original problem into a series of subproblems to efficiently solve the original optimization problem. We further derive a two-type sub-algorithm, which uses the BFGS algorithm to solve convex subproblems and employ the SQP-based algorithm to deal with non-convex subproblems.
- The convergence of the proposed algorithm is discussed. A series of simulation experiments have been conducted to explore the influence of multi-platoon dynamic characteristics and other parameters on system performance. The results demonstrate that the proposed algorithm outperforms a group of benchmark schemes, which applies to the case when the number of multi-platoon vehicles, time slots, and other simulation parameters change.

The rest of this paper is organized as follows. We formulate the UAV-enabled MEC system model and the energy efficiency maximization problem in Section II. In Section III, an algorithm for the non-convex problem is proposed. Section IV shows the simulation results to evaluate the performance of the proposed algorithm, and Section V concludes our paper and outlines the future work.

II. System Model

As shown in Fig. 1, a UAV-aided system is formulated, in which a UAV equipped with MEC server provides computation and communication services to turning platooning vehicles. The platooning vehicle nodes, for example, the ground user nodes, are denoted by $V(m)$, where m ranges from 1 to M, and M represents the number of vehicles. The UAV is denoted by U, and in our model, the number of UAV remains 1. For convenience of exposition, we discretize the finite passing time T into N equal-time slots, i.e., $T = N \cdot \tau$, and n is the time slots index ($0 \leq n \leq N$, n is an integer). According to existing literature [14], [31], [32], in order to eliminate mutual interference among wireless offloading processes of multi-user communication, we adopt the Time Division Multiple Access (TDMA) protocol in our paper. The interaction time interval between vehicle m ($1 \leq m \leq M$) and the UAV during the nth ($1 \leq n \leq N$) time slot, is denoted by $t_m[n] (0 \leq t_m[n] \leq \tau)$. Further, for the interaction time for each vehicle $t_m[n]$, we divide it into three parts, which would be processed by turn, that is, the computation offloading time $t_m^o[n]$ of vehicle m, the task

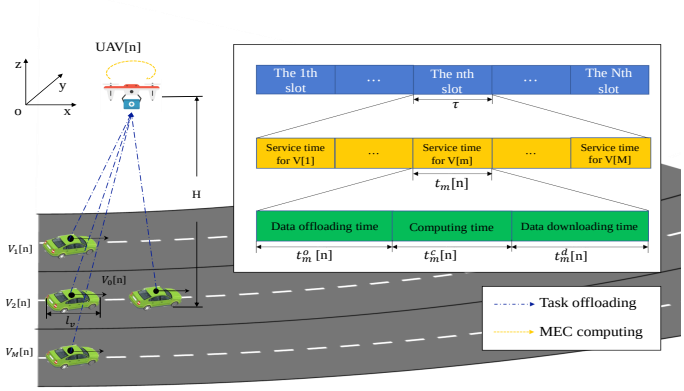

Fig. 1: A typical application scenario of the UAV-MEC assisted turning formation vehicles system. The total service time of each vehicle is the sum of communication and calculation times.

computing time $t_m^c[n]$ of the UAV, and the results downloading time $t_m^d[n]$. We also established a 3D Cartesian coordinate system, thus the location coordinates of vehicles and UAV at time slot n can be denoted by $\mathbf{q}^v[n] = [x[n], y[n], z[n]]$ and $\mathbf{q}^u[n] = [x[n], y[n], z[n]]$, while the vehicles' height remains 0 and the UAV's flight altitude is fixed to H ($H > 0$). Because the flight height span of UAV is relatively small compared with horizontal distance, thus the impact of height change on the G2A communication channel and resource scheduling can be ignored and the height of UAV can be simplified as a fixed value according to existing literature [14], [27], [33]. In the next part, we formulate the system model in terms of mobility, communication, computation, and energy efficiency.

A. Mobility Model

Existing literature [27], [34], [35] focuses on optimizing the problem with low user mobility. Nevertheless, the original considerations seem impractical when it comes to vehicle users, and another literature assumes the vehicles move along a straight line [13]. Our research considers vehicle turning scenarios with platooning vehicles, which is widespread in the applications of intelligent vehicle control technology and ADAS.

Moreover, to imitate the driving behavior of real drivers, the acceleration of a specific vehicle depends on the difference between the predetermined desired position and speed difference and the position and speed difference of this vehicle's preceding vehicle. Therefore, while establishing a driver model, we have introduced Frenet to simplify the control process.

Frenet is a coordinate system that takes the centerline of the road as the X axis and the normal road as the Y axis [36]. Thus, for intelligent vehicle platooning scenarios, vertical motion can be ignored and simplified as plane motion. In this scenario, the Frenet coordinate system refers to the curve tangent vector $\mathbf{T}$, and the normal vector $\mathbf{N}$ constitutes a right-handed rectangular coordinate system that moves along the reference curve. Thus, the (s, l) in the Frenet coordinate system can be transformed to (x, y) in the Cartesian coordinate

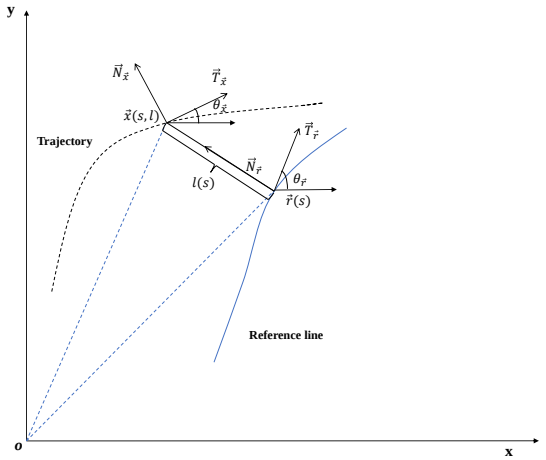

Fig. 2: A Schematic diagram of conversion between Frenet coordinates and Cartesian coordinates.

system as follows:

$$\begin{cases} x_m[n] = x_m^{\vec{r}}[n] - l_m[n]\sin\theta_m^{\vec{r}}[n]; \\ y_m[n] = y_m^{\vec{r}}[n] + l_m[n]\cos\theta_m^{\vec{r}}[n]; \\ \theta_m[n] = \tan^{-1}\left(\dfrac{l'_m[n]}{1-k_m^{\vec{r}}[n]l_m[n]}\right) + \theta_m^{\vec{r}}[n]; \\ v_m[n] = \sqrt{[\dot{s}_m[n](1-k_m^{\vec{r}}[n]l_m[n])]^2 + (\dot{s}_m[n]l'_m[n])^2}; \\ a_m[n] = \ddot{s}_m[n]\dfrac{1-k_m^{\vec{r}}[n]l_m[n]}{\cos(\theta_m[n]-\theta_m^{\vec{r}}[n])} + [l'_m[n](k_m[n] \\ \qquad \dfrac{1-k_m^{\vec{r}}[n]l_m[n]}{\cos(\theta_m[n]-\theta_m^{\vec{r}}[n])} - k_m^{\vec{r}}[n]) - (k_m^{\vec{r}}{}'[n] \\ \qquad l_m[n] + k_m^{\vec{r}}[n]l'_m[n])]\dfrac{\dot{s}_m[n]^2}{\cos(\theta_m[n]-\theta_m^{\vec{r}}[n])}; \\ k_m[n] = \dfrac{\cos(\theta_m[n]-\theta_m^{\vec{r}}[n])}{1-k_m^{\vec{r}}[n]l_m[n]}\left\{\left[l''_m[n] + \left(k_m^{\vec{r}}{}'[n]\right.\right.\right. \\ \qquad \left.\left.\left. l_m[n] + k_m^{\vec{r}}[n]l'_m[n]\right)\right]\dfrac{\cos^2(\theta_m[n]-\theta_m^{\vec{r}}[n])}{1-k_m^{\vec{r}}[n]l_m[n]} \\ \qquad +k_m^{\vec{r}}[n]\right\}. \end{cases} \tag{1}$$

As shown in Fig. 2, s and l are the tangential and normal coordinates of the vehicle in the Frenet coordinate system [36]. Likewise, $x^{\vec{r}}$ and $y^{\vec{r}}$ are the corresponding Cartesian horizontal and vertical axes of the matching point at the reference line, and $\theta^{\vec{r}}$ is its direction angle at that point. The variable $k^{\vec{r}}$ is the curvature of the matching point, and $k^{\vec{r}'}$ is its derivative to the Frenet normal coordinate. The corresponding parameters of the actual vehicle position are x, y, θ and k. The variables v and a are the velocity and acceleration of the target vehicle. The symbol l' denotes the derivative of the Frenet normal axis to its tangential axis, and l'' represents the second derivative of the normal axis to the tangential axis of the Frenet coordinate system. The first and second derivatives of the Frenet tangential coordinate with respect to time are designated as $\dot{s}$ and $\ddot{s}$.

A specific platooning vehicle generates its acceleration by evaluating the speed difference, position difference between

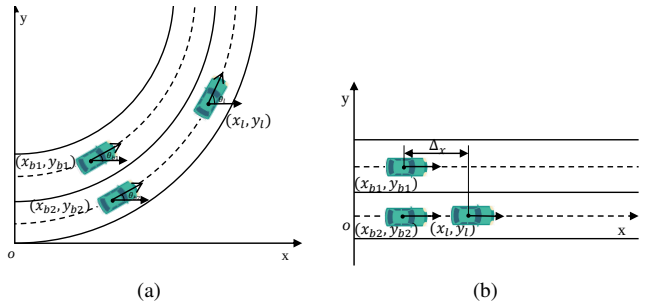

Fig. 3: Platooning vehicles under different coordinate system. (a) the Cartesian coordinate system. (b) the Frenet coordinate system.

the vehicle ahead, and the expected speed difference and position difference, thereby maintaining the vehicles' formation and stability. From Fig. 3, the Frenet coordinate system transforms the two-dimensional motion into one-dimensional, which simplifies the control process related to the heading angle θ. The platooning vehicles studied in this paper do not change lanes during the driving process, because according to most countries' traffic safety regulations (for example, China), vehicles are not allowed to change lanes when turning in the area of sharp turn or tunnels to avoid accidents.

The vehicles adopt a leader-follower strategy in a formation, in which the speed v_0 and acceleration a_0 of the leader vehicle have been predetermined. Let the acceleration of follower m in slot n be $a_m[n]$. It can be determined with expected speed $v_m^e[n]$, expected $\triangle_m^e[n-1]$ and actual $\triangle_m[n-1]$ position differences, and actual velocity $v_m[n-1]$ as follows:

$$a_m[n] = k_1\left(v_m^e[n] - v_m[n-1]\right), \tag{2}$$

where $v_m^e[n]$ can be determined as follows:

$$v_m^e[n] = v_m[n-1] + k_2\triangle_m^e[n-1] - \triangle_m[n-1]. \tag{3}$$

The parameters k_1 and k_2 in the above formula are the control gain parameters.

It is widely assumed that in different time slots [4], [13], the vehicles movement can be simplified to a uniform acceleration movement. Hence, its motion equation can be expressed as follows:

$$\begin{cases} v_m[n] = v_m[n-1] + a_m[n]\tau, \\ x_m[n] = x_m[n-1] + v_m[n-1]\tau + \dfrac{1}{2}a_m[n]\tau^2. \end{cases} \tag{4}$$

B. Communication Model

According to the existing literature [13], [27], [33], [35], as the altitude of UAV is much higher than that of vehicles, Since the LoS (line of sight) channel of the UAV communication links are much more predominant than other channel impairments, and it is considered deployed in an open environment, thus the UAV-to-ground communication channel can be considered as an LoS channel. And the Doppler frequency shift caused by mobility is assumed to be compensated at the receivers [27], [33], [37].

The channel remains unchanged for a finite flying time. Thus the channel power gain between the UAV and the ground vehicle nodes can be expressed as follows:

$$g_m[n] = \frac{g_0}{H^2 + \|\mathbf{q}^v[n] - \mathbf{q}^u[n]\|^2}, \tag{5}$$

where g_0 indicates the channel power gain at a reference distance d_0 = 1 m.

Suppose the available communication bandwidth is B, and the power used by the vehicle for upstream offloading at slot n is $P_m[n]$, the bytes of data transmitted upstream $R_m[n]$ can be expressed according to Shannon's formula as:

$$R_m[n] = B\log_2(\frac{P_m[n]\, g_m[n]}{N_0} + 1), \tag{6}$$

The communication energy consumption of vehicles is represented with the function $E_m^o[n]$:

$$E_m^o[n] = P_m[n]\, t_m^o[n], \tag{7}$$

where N_0 is the noise power, and $t_m^o[n]$ denotes the data transmission time of vehicle node m at slot n.

To ensure users' QoS, the total offloading data rate in time slot n shall not be lower than the allowed minimum transmission data bits $\underline{\mathrm{R}}[n]$:

$$\sum_{m=1}^{M} R_m[n] \geq \underline{\mathrm{R}}[n]. \tag{8}$$

C. Computation Model

Our paper assumes that the drone node employs the binary computation mode, that is, each computation task has to be executed as a whole. For example, when the task is highly integrated or relatively simple, its correlated data cannot be partitioned and has to be performed as a whole [6]. And the UAV carries out all the task calculations using a constant CPU cycle f. Letting C denotes the CPU frequency needed for computation process per bit, the UAV's computational time m in slot n, $t_m^c[n]$ can be formulated as follows:

$$t_m^c[n] = \frac{R_m[n] t_m^o[n] C}{f}. \tag{9}$$

Its consumed energy is represented by $E_m^c[n]$ according to existing literature [4], [15], [30]:

$$E_m^c[n] = \lambda f^3 t_m^c[n], \tag{10}$$

where λ is the effective capacitance coefficient of the UAV's processor chip.

Since the downlink transmission process is ignored, the constraint of $t_m^o[n]$ and $t_m^c[n]$ can be proposed as follows:

$$\sum_{m=1}^{M} (t_m^c[n] + t_m^o[n]) \leq \tau. \tag{11}$$

D. Energy Efficiency Optimization Model

Because of the limited energy available to the unmanned aerial vehicle, the UAV's consumed energy in the computation process should meet the following energy constraints, given as:

$$\sum_{m=1}^{M}\sum_{n=1}^{N} \lambda f^3 t_m^c[n] \leq \widetilde{E}, \tag{12}$$

where $\widetilde{E}$ is the maximum energy stored in the UAV's battery.

Each vehicle's total energy consumption (including communication energy consumption and computing energy consumption) E_m^{veh} can be formulated as:

$$E_m^{veh}(t_m^c[n], P_m[n]) = \sum_{n=1}^{N} E_m^c[n] + \sum_{n=1}^{N} E_m^o[n]. \tag{13}$$

The total offloaded data R_m^{veh} of vehicle m is expressed as:

$$R_m^{veh}(t_m^o[n], P_m[n]) = \sum_{n=1}^{N} t_m^o[n] R_m[n]. \tag{14}$$

Therefore, the energy efficiency EE_m^{veh} of vehicle m can be formulated as follows:

$$\begin{aligned} &EE_m^{veh}(t_m^o[n], t_m^c[n], P_m[n], \eta) \\ &= \frac{R_m^{veh}(t_m^o[n], P_m[n])}{E_m'^{veh}(t_m^c[n], P_m[n], \eta)} \\ &= \frac{\sum_{n=1}^{N} t_m^o[n] R_m[n]}{\sum_{n=1}^{N} E_m^c[n] + \eta \sum_{n=1}^{N} E_m^o[n]}, \end{aligned} \tag{15}$$

where η is the weight factor of the energy consumption of vehicle nodes, and $E_m'^{veh}$ is the adjusted communication and computation energy, which can be adjusted to address the preference of energy consumption according to the practical system.

In addition to the weight parameter η for communication energy consumption, a weight vector Wei_{veh} for vehicle platoon is designed to show the preferences for the energy efficiency of different vehicles.

$$Wei_{veh} = [Wei_1, Wei_2, ..., Wei_M], \tag{16}$$

where the sum of all elements of Wei_{veh} remains 1. In the experiments of this paper, when the number of vehicles is greater than 1, the weight of the leading vehicle are kept constant (when the number of vehicles is 1, the weight matrix is 1), and the remaining weights would be assigned to the following vehicles.

The energy efficiency vector of vehicle platoon is represented by EE_{veh}.

$$EE_{veh} = [EE_1^{veh}, EE_2^{veh}, ..., EE_M^{veh}], \tag{17}$$

thus the energy efficiency of the vehicle platoon can be expressed as follows:

$$EE_{sys}(t_m^o[n], t_m^c[n], P_m[n], \eta) = Wei_{veh} EE_{veh}. \tag{18}$$

In this UAV-enabled MEC system, we jointly optimized the data transmission time and transmission power to maximize the total energy efficiency. The objective function is given as $EE_{sys}(\mathbf{x})$, where $\mathbf{x}$ is a vector that represents the variables,

including communication power P_m and time t_m^o to be optimized. The problem can be framed as $P1$:

$$\begin{aligned} P1: \max_{\mathbf{x}}: & \ EE_{sys}(\mathbf{x}) && \text{(19a)}\\ \text{s.t.}&(8),(9),(11),(12), && \text{(19b)}\\ & 0 \le P_m[n] \le P_{max}, && \text{(19c)}\\ & 0 \le t_m^o[n], t_m^c[n] \le \tau, && \text{(19d)}\\ & m = 1,\ldots,M;\ n = 1,\ldots,N, && \text{(19e)} \end{aligned}$$

where P_{max} is the maximum transmission power of vehicle nodes. (8) denotes the QoS constraint, which is used to ensure the minimum computing requirements for vehicle platoon in each time slot. Limited to battery capacity, the computation energy consumption of the UAV should be lower than a specific boundary, which is expressed by the constraint (12). The expressions (19c) and (19d) are the boundary constraints of the transmission power, and the transmission time and computation time, respectively.

The above problem is highly non-convex due to the strong coupling between variables and the complexity of the objective function. It would be somewhat costly to solve the above problem directly. Therefore, an efficient algorithm is proposed to solve $P1$, proven to converge to the local optimum.

III. Joint Optimization Method

In this section, we first rearrange problem $P1$'s equality and inequality constraints and turn it into a simplified form $P2$. Then, based on the interior-point algorithm, we transform the expanded problem into a series of approximate optimization subproblems and apply two optimization sub-algorithms to solve them based on their convexity or non-convexity.

A. Approximate Subproblem Formulation

We use the concept of an external penalty function for equality constraints and an obstacle function for inequality constraints to construct a hybrid augmented objective function whose purpose is to eliminate constraints. We can denote equalities and inequalities by $c_i(\mathbf{x}) = 0$ and $c_j'(\mathbf{x}) \ge 0$, respectively. Also, we can represent the indexes of equality and inequality constraints with $\mathbb{I}$ and $\mathbb{J}$, noting that the total number of the constraints is NM and $4NM + 2N + 1$, respectively. Thus, the problem $P1$ can be simplified. In particular, we introduce the slack variable $z_j,\ j = 1, 2, \ldots, 4NM+2N+1$, to make the initial point selection easier and equivalently transform the problem $P1$ into $P2$ [38]:

$$\begin{aligned} P2: \min_{\mathbf{x}}: & -EE_{sys}(\mathbf{x}) \\ \text{s.t.} & \begin{cases} c_i(\mathbf{x}) = 0, i \in \mathbb{I}, \\ c_j'(\mathbf{x}) - z_j = 0, j \in \mathbb{J}, \\ z_j \ge 0, j \in \mathbb{J}. \end{cases} \end{aligned} \tag{20}$$

Then the mixed augmented objective function $\varphi(\mathbf{x}, \mathbf{z}, \mu)$ of the equivalent problem $P2$ is constructed as follows [39], $\mu\ (\mu > 0)$ is the penalty factor used to construct the augmented objective function:

$$\begin{aligned} P3: \varphi(\mathbf{x}, \mathbf{z}, \mu) = & -EE_{sys}(\mathbf{x}) + \frac{1}{2\mu}\sum_{i=1}^{NM} c_i^2(\mathbf{x}) \\ & + \frac{1}{2\mu}\sum_{j=1}^{4NM+2N+1}\left[c_j'(\mathbf{x}) - z_j\right]^2 \\ & + u\sum_{j=1}^{4NM+2N+1}\frac{1}{z_j}. \end{aligned} \tag{21}$$

At this point, any $(\mathbf{x}, \mathbf{z})(x_i, z_j > 0)$ can be used as an appropriate initial point to start the corresponding iterative algorithm. The penalty function part of the augmented objective function $\varphi(\mathbf{x}, \mathbf{z}, \mu)$ is called the barrier function and it is denoted by $\bar{\varphi}(\mathbf{x}, \mathbf{z}, \mu)$:

$$\begin{aligned} \bar{\varphi}(\mathbf{x}, \mathbf{z}, \mu) = & \frac{1}{2\mu}\sum_{i=1}^{NM} c_i^2(\mathbf{x}) + \frac{1}{2\mu}\sum_{j=1}^{4NM+2N+1}\left[c_j'(\mathbf{x}) - z_j\right]^2 \\ & + u\sum_{j=1}^{4NM+2N+1}\frac{1}{z_j}. \end{aligned} \tag{22}$$

On this basis, we can use a series of optimization sub-algorithms to solve the above optimization subproblem.

B. Approximate Subproblem Optimization Algorithms

Two types of optimization algorithms are employed to solve the approximate subproblems iteratively: the BFGS-Armijo method and the sequential quadratic programming (SQP)-based method [40]. The choice depends on the subproblem convexity. When the approximate subproblem is locally non-convex, it takes the SQP-based step. Otherwise, it uses the BFGS-Armijo step.

1) BFGS-Armijo Method: The basic idea of using iterative algorithms to solve approximate subproblems is to give an initial point and then generate an iterative sequence according to a particular iterative rule. The update process of the iteration point column is as follows:

$$\mathbf{x}_{k+1} = \mathbf{x}_k + \alpha_k \mathbf{d}_k, \tag{23}$$

where $\mathbf{x}_k$ is the kth iteration point, $\mathbf{d}_k$ is the kth search direction, and α_k is the kth step size in the direction $\mathbf{d}_k$.

Here, we employ the BFGS algorithm to construct the positive definite Hessian approximation matrix $\mathbf{B}_k$ of the problem's objective function to obtain the search direction. And k represents the kth iterative step of the subproblem $P3$. Then, an imprecise line-search method is exploited to determine the appropriate step size. Finally, the $\mathbf{B}_k$ can be obtained through the information of the previous step.

$$\mathbf{B}_{k+1} = \mathbf{B}_k - \frac{\mathbf{B}_k \mathbf{s}_k \mathbf{s}_k^T \mathbf{B}_k}{\mathbf{s}_k^T \mathbf{B}_k \mathbf{s}_k} + \frac{\mathbf{y}_k \mathbf{y}_k^T}{\mathbf{y}_k^T \mathbf{s}_k}, \tag{24}$$

where $\mathbf{s}_k$ is the displacement defined as $\mathbf{s}_k = \mathbf{x}_{k+1} - \mathbf{x}_k$, and $\mathbf{y}_k$ is the difference of the gradient between kth step and $(k+1)th$ step.

$$\mathbf{y}_k = \nabla_{(\mathbf{x},\mathbf{z})}(\varphi(\mathbf{x}_{k+1},\mathbf{z}_{k+1},\mu)) - \nabla_{(\mathbf{x},\mathbf{z})}(\varphi(\mathbf{x}_k,\mathbf{z}_k,\mu)). \quad (25)$$

Feasible search direction $\mathbf{d}_k$ can be obtained by solving the following linear equations.

$$\mathbf{B}_k\mathbf{d}_k = -\nabla_{(\mathbf{x},\mathbf{z})}(\varphi(\mathbf{x}_k,\mathbf{z}_k,\mu)). \quad (26)$$

Based on (24), we can get the following results.

Lemma 1: Suppose $\mathbf{B}_k$ is symmetric positive definite, and $\mathbf{B}_{k+1}$ is determined by equation (24), then the necessary and sufficient condition for $\mathbf{B}_{k+1}$ to be symmetric positive definite is $\mathbf{y}_k^T\mathbf{s}_k > 0$.

Proof: The necessity of Lemma 1 is obvious, because $\mathbf{y}_k^T\mathbf{s}_k = \mathbf{s}_k^T\mathbf{B}_{k+1}\mathbf{s}_k$. If $\mathbf{B}_{k+1}$ is positive definite, then clearly there is $\mathbf{y}_k^T\mathbf{s}_k > 0$. The sufficiency will be proved in the following paragraph. Suppose that $\mathbf{y}_k^T\mathbf{s}_k > 0$ and $\mathbf{B}_k$ is positive definite, then according to (24), for any $\mathbf{d} \in \mathbb{R}^n$ and $\mathbf{d} \neq 0$, it holds that:

$$\mathbf{d}^T\mathbf{B}_{k+1}\mathbf{d} = \mathbf{d}^T\mathbf{B}_k\mathbf{d} - \frac{(\mathbf{d}^T\mathbf{B}_k\mathbf{s}_k)^2}{\mathbf{s}_k^T\mathbf{B}_k\mathbf{s}_k} + \frac{(\mathbf{d}^T\mathbf{y}_k)^2}{\mathbf{y}_k^T\mathbf{s}_k}. \quad (27)$$

Because $\mathbf{B}_k$ is a symmetric and positive definite matrix, there is a symmetric positive definite matrix $\mathbf{B}_k{}^{\frac{1}{2}}$. Therefore, $\mathbf{B}_k$ can be expressed as $\mathbf{B}_k = \mathbf{B}_k{}^{\frac{1}{2}}\mathbf{B}_k{}^{\frac{1}{2}}$. In the following formula, the Cauchy-Schwartz inequality is used to obtain the results:

$$\begin{aligned}(\mathbf{d}^T\mathbf{B}_k\mathbf{s}_k)^2 &= [(\mathbf{B}_k{}^{\frac{1}{2}}\mathbf{d})^T(\mathbf{B}_k{}^{\frac{1}{2}}\mathbf{s}_k)]^2 \\ &\leq \|\mathbf{B}_k{}^{\frac{1}{2}}\mathbf{d}\|^2\|\mathbf{B}_k{}^{\frac{1}{2}}\mathbf{s}_k\|^2 \\ &= (\mathbf{B}_k{}^{\frac{1}{2}}\mathbf{d})^T(\mathbf{B}_k{}^{\frac{1}{2}}\mathbf{d})(\mathbf{B}_k{}^{\frac{1}{2}}\mathbf{s}_k)^T(\mathbf{B}_k{}^{\frac{1}{2}}\mathbf{s}_k) \\ &= (\mathbf{d}^T\mathbf{B}_k\mathbf{d})(\mathbf{s}_k^T\mathbf{B}_k\mathbf{s}_k).\end{aligned} \quad (28)$$

According to (27) and (28), it can be concluded that $[(\mathbf{B}_k{}^{\frac{1}{2}}\mathbf{d})^T(\mathbf{B}_k{}^{\frac{1}{2}}\mathbf{s}_k)]^2 = \|\mathbf{B}_k{}^{\frac{1}{2}}\mathbf{d}\|^2\|\mathbf{B}_k{}^{\frac{1}{2}}\mathbf{s}_k\|^2$, and if there is a real number $\tau_k \neq 0$ that makes $\mathbf{B}_k{}^{\frac{1}{2}}\mathbf{d} = \tau_k\mathbf{B}_k{}^{\frac{1}{2}}\mathbf{s}_k$, that is, $\mathbf{d} = \tau_k\mathbf{s}_k$, and vice versa.

$$\begin{aligned}\mathbf{d}^T\mathbf{B}_{k+1}\mathbf{d} &\geq \mathbf{d}^T\mathbf{B}_k\mathbf{d} - \frac{(\mathbf{d}^T\mathbf{B}_k\mathbf{d})(\mathbf{s}_k^T\mathbf{B}_k\mathbf{s}_k)}{\mathbf{s}_k^T\mathbf{B}_k\mathbf{s}_k} + \frac{(\mathbf{d}^T\mathbf{y}_k)^2}{\mathbf{y}_k^T\mathbf{s}_k} \\ &= \frac{(\mathbf{d}^T\mathbf{y}_k)^2}{\mathbf{y}_k^T\mathbf{s}_k} > 0.\end{aligned} \quad (29)$$

Therefore, for any $\mathbf{d} \in \mathbb{R}^n, \mathbf{d} \neq 0$, if $\mathbf{y}_k^T\mathbf{s}_k > 0$, then it holds that $\mathbf{d}^T\mathbf{B}_{k+1}\mathbf{d} > 0$ which proves Lemma 1. ∎

Given the fact that the Armijo line-search criterion cannot guarantee $\mathbf{y}_k^T\mathbf{s}_k > 0$, the update formula of $\mathbf{B}_k$ can be adjusted to ensure the symmetric positive definiteness of matrix sequence $\mathbf{B}_k$ when the criterion is adopted. Thus, we can solve the feasible research direction $\mathbf{d}_k$ using (24) and (26).

$$\mathbf{B}_{k+1} = \begin{cases} \mathbf{B}_k, \ \mathbf{y}_k^T\mathbf{s}_k \leq 0; \\ \mathbf{B}_k - \frac{\mathbf{B}_k\mathbf{s}_k\mathbf{s}_k^T\mathbf{B}_k}{\mathbf{s}_k^T\mathbf{B}_k\mathbf{s}_k} + \frac{\mathbf{y}_k\mathbf{y}_k^T}{\mathbf{y}_k^T\mathbf{s}_k}, \ \mathbf{y}_k^T\mathbf{s}_k > 0. \end{cases} \quad (30)$$

According to the Armijo criterion, the appropriate step size α_k can be approximated with the following formula:

$$\alpha_k = \beta^{\xi_k}, \quad (31)$$

Algorithm 1: The interior-point-based method for $P1$

1: Settings:
tolerance error $0 \leq \varepsilon \ll 1$, penalty factor reduction coefficient $\rho \in (0,1)$, $\widetilde{E}$, T, N and other factors;
2: Initialization:
initialize point $\mathbf{x}_0 \in \mathbb{D}_0$ and penalty factor $\mu_1 > 0$;
3: Repeat 1:
transform original problem to subproblem $P3$ or $P4$;
initialize the iterative number $i = 1$;
Repeat 2:
initialize the iterative number $k = 1$;
obtain $\mathbf{x}_{i+1}$,$\mathbf{z}_{i+1}$ by solving subproblem $P3$ or $P4$ for given μ_i;
if subproblem $P3$ is convex
initialize tolerance error $0 \leq \delta_i \ll 1$;
solve subproblem $P3$ through BFGS-Armijo steps;
update $k = k + 1$;
if $\|\nabla\varphi(\mathbf{x}_k,\mathbf{z}_k,\mu_i)\| \leq \delta_i$
$\mathbf{x}_{i+1} = \mathbf{x}_k, \ \mathbf{z}_{i+1} = \mathbf{z}_k$;
break;
end
else
initialize tolerance error $0 \leq \delta_i' \ll 1$;
solve subproblem $P4$ through SQP-based steps;
update $k = k + 1$;
if $O(\mathbf{x}_k,\mathbf{z}_k,\mu) \leq \delta_i'$
$\mathbf{x}_{i+1} = \mathbf{x}_k$ and $\mathbf{z}_{i+1} = \mathbf{z}_k$;
break;
end
end
end Repeat 2
update $\mu_{i+1} = \rho \cdot \mu_i$ and iterative number $i = i + 1$;
if $\mu_i\bar{\varphi}(\mathbf{x},\mathbf{z}) \leq \varepsilon$
the maximum energy efficiency EE_{sys}^{opt} is obtained;
break;
end
end Repeat 1
4: Obtain solutions:
P_m^{opt} and $t_m^{opt,o}$.

$\beta \in (0,1)$ is a predetermined parameter and ξ_k is the smallest non-negative integer that satisfies the following inequalities:

$$\varphi\left((\mathbf{x}_k,\mathbf{z}_k,\mu_k) + \beta^{\xi_k}\mathbf{d}_k\right) \leq \varphi(\mathbf{x}_k,\mathbf{z}_k,\mu_k) + \sigma\beta^{\xi_k}\mathbf{y}_k^T\mathbf{d}_k, \quad (32)$$

where σ is a predetermined parameter and $\sigma \in (0, 0.5)$.

2) The SQP-based Method: It takes the SQP-based step when the approximate subproblem is not locally convex. This step minimizes a quadratic approximation to the approximate problem using the trust region method [40], [41].

At this point, we reformulate the problem to the following form, and μ is the penalty factor and $\mu > 0$:

$$\begin{aligned}P4: \min_{\mathbf{x},\mathbf{z}}: &-EE_{sys}(\mathbf{x}) + \mu \sum_{j=1}^{4NM+2N+1} \frac{1}{z_j} \\ \text{s.t.} &\begin{cases} c_i(\mathbf{x}) = 0, i \in \mathbb{I}, \\ c_j'(\mathbf{x}) - z_j = 0, j \in \mathbb{J}. \end{cases}\end{aligned} \quad (33)$$

Slack variables z_j are restricted to positive to keep the interior iterates of the feasible region. We can use $\Phi(\mathbf{x})$ and $\mathbf{c}(\mathbf{x})$ to represent the objective function and the constraints, respectively. The resulting problem can be rewritten as:

$$\begin{aligned} P4' : \min_{\mathbf{x},\mathbf{z}} &: \Phi(\mathbf{x},\mathbf{z}) \\ \text{s.t. } &\mathbf{c}(\mathbf{x},\mathbf{z}) = \mathbf{0}. \end{aligned} \tag{34}$$

To deal with the non-convexity, we apply the SQP method to transform the problem $P4'$ into the following quadratic problem. A feasible search direction $\mathbf{d}_k$ at kth step is obtained:

$$\begin{aligned} P5 : \min_{\mathbf{d}_k} &: \nabla\Phi(\mathbf{x}_k,\mathbf{z}_k)^T\mathbf{d}_k + \frac{1}{2}\mathbf{d}_k^T\mathbf{W}_k\mathbf{d}_k \\ \text{s.t. } &\hat{\mathbf{A}}(\mathbf{x}_k,\mathbf{z}_k)^T\mathbf{d}_k + \mathbf{c}(\mathbf{x}_k,\mathbf{z}_k) = \mathbf{0}, \end{aligned} \tag{35}$$

where $\mathbf{W}_k$ is the Hessian of $L(\mathbf{x}_k,\mathbf{z}_k,\lambda_k^{\mathbf{c}})$ (the Lagrangian function of the problem $P4'$), $\hat{\mathbf{A}}(\mathbf{x}_k,\mathbf{z}_k)^T$ is the Jacobian of $\mathbf{c}(\mathbf{x}_k,\mathbf{z}_k)$ and $\lambda_k^{\mathbf{c}}$ are the Lagrange multipliers. $\nabla\Phi(\mathbf{x}_k,\mathbf{z}_k)$ represents the Jacobi matrix of the objective function. Considering $\mathbf{W}$ may be non-positive definite within the null space of $\hat{\mathbf{A}}$, a trust region constraint is employed [40] (we decompose $\mathbf{d}_k$ into $[\mathbf{d}_k^{\mathbf{x}},\mathbf{d}_k^{\mathbf{z}}]$):

$$\begin{bmatrix} \mathbf{d}_k^{\mathbf{x}} \\ \mathbf{Z}_k^{-1}\mathbf{d}_k^{\mathbf{z}} \end{bmatrix} \le \triangle_k, \tag{36}$$

where $\triangle_k$ is the radius of the trust region, which would be updated at each iteration and $\mathbf{Z} = \mathrm{diag}[z_1,...z_j]$.

Furthermore, to ensure the positivity of $\mathbf{z}$, we introduce a constraint of $\mathbf{d}_k^{\mathbf{z}}$:

$$\mathbf{z}_k + \mathbf{d}_k^{\mathbf{z}} \ge (1-\omega)\mathbf{z}_k. \tag{37}$$

The parameters ω is less than 1 but close to it. Thus, we can formulate subproblem $P6$:

$$\begin{aligned} P6 : \min_{\mathbf{d}_k} &: \nabla\Phi(\mathbf{x}_k,\mathbf{z}_k)^T\mathbf{d}_k + \frac{1}{2}\mathbf{d}_k^T\mathbf{W}_k\mathbf{d}_k \\ \text{s.t. } &\begin{cases} \hat{\mathbf{A}}(\mathbf{x}_k,\mathbf{z}_k)^T\mathbf{d}_k + \mathbf{c}(\mathbf{x}_k,\mathbf{z}_k) = \mathbf{0}, \\ \begin{bmatrix} \mathbf{d}_k^{\mathbf{x}} \\ \mathbf{Z}_k^{-1}\mathbf{d}_k^{\mathbf{z}} \end{bmatrix} \le \triangle_k, \\ \mathbf{d}_k^{\mathbf{z}} \ge -\omega\cdot\mathbf{z}_k. \end{cases} \end{aligned} \tag{38}$$

However, since the step size that satisfies the linear constraint may not be in the trust region, we need to solve the subproblem $P6.1$ to find a standard step size $\mathbf{v}$ [40] that is in the region and meets the constraints as much as possible.

$$\begin{aligned} P6.1 : \min_{\mathbf{v}_k} &: \|\hat{\mathbf{A}}(\mathbf{x}_k,\mathbf{z}_k)^T\mathbf{v}_k + \mathbf{c}(\mathbf{x}_k,\mathbf{z}_k)\| \\ \text{s.t. } &\begin{cases} \begin{bmatrix} \mathbf{v}_k^{\mathbf{x}} \\ \mathbf{Z}_k^{-1}\mathbf{v}_k^{\mathbf{z}} \end{bmatrix} \le \epsilon\triangle_k, \\ \mathbf{v}_k^{\mathbf{z}} \ge -\omega\cdot\mathbf{z}_k, \end{cases} \end{aligned} \tag{39}$$

where ϵ is the contraction parameter and $0<\epsilon<1$. Then, we use the found step size to calculate $\mathbf{d}_k$ ($\mathbf{d}_k = \mathbf{x}_{k+1} - \mathbf{x}_k$) in $P6.2$.

$$\begin{aligned} P6.2 : \min_{\mathbf{d}_k} &: \nabla\Phi(\mathbf{x}_k,\mathbf{z}_k)^T\mathbf{d}_k + \frac{1}{2}\mathbf{d}_k^T\mathbf{W}_k\mathbf{d}_k \\ \text{s.t. } &\begin{cases} \hat{\mathbf{A}}(\mathbf{x}_k,\mathbf{z}_k)^T\mathbf{d}_k = \hat{\mathbf{A}}(\mathbf{x}_k,\mathbf{z}_k)^T\mathbf{v}_k, \\ \begin{bmatrix} \mathbf{d}_k^{\mathbf{x}} \\ \mathbf{Z}_k^{-1}\mathbf{d}_k^{\mathbf{z}} \end{bmatrix} \le \triangle_k, \\ \mathbf{d}_k^{\mathbf{z}} \ge -\omega\cdot\mathbf{z}_k. \end{cases} \end{aligned} \tag{40}$$

To decide if step $\mathbf{d}_k$ obtained above should be accepted, we introduce a merit function $\phi(\mathbf{x}_k,\mathbf{z}_k,\zeta)$. The merit function is defined as follows [40]:

$$\phi(\mathbf{x}_k,\mathbf{z}_k,\zeta) = \Phi(\mathbf{x}_k,\mathbf{z}_k) + \zeta\|c(\mathbf{x}_k,\mathbf{z}_k)\|, \tag{41}$$

where $\zeta>0$ is a penalty parameter. And if step $\mathbf{d}_k$ satisfies the following formula, then the step size $\mathbf{d}_k$ will be accepted:

$$\triangle\phi = \Phi(\mathbf{x}_k+\mathbf{d}_k^{\mathbf{x}},\mathbf{z}_k+\mathbf{d}_k^{\mathbf{z}},\zeta) - \Phi(\mathbf{x}_k,\mathbf{z}_k,\zeta) \ge \kappa, \tag{42}$$

where κ is the tolerance reduction. Otherwise, we should decrease the trust region radius $\triangle_k$ and the algorithm will go to $P6.1$.

Rather than solving subproblem $P6$ accurately, the algorithm will stop when approximate solution $(\hat{\mathbf{x}},\hat{\mathbf{z}})$ satisfies $O(\hat{\mathbf{x}},\hat{\mathbf{z}},\mu)\le\delta'$, and δ' denotes the tolerance error. $O(\mathbf{x},\mathbf{z},\mu)$ measures the optimality conditions of the barrier problem and is defined as follows [41]:

$$\begin{aligned} O(\mathbf{x},\mathbf{z},\mu) = \max(&\|\nabla(-EE_{sys}(\mathbf{x})) + \mathbf{A}^{\mathbf{c}}(\mathbf{x})\lambda^{\mathbf{c}}\|_\infty, \\ &\|\mathbf{Z}\lambda^{\mathbf{c}'} - \mu\mathbf{e}\|_\infty, \|\mathbf{c}(\mathbf{x})\|_\infty, \|\mathbf{c}'(\mathbf{x})+\mathbf{z})\|_\infty), \end{aligned} \tag{43}$$

where $\mathbf{e} = [1,...1]^T$, $\mathbf{Z} = \mathrm{diag}(z_1,...,z_j)$. $\mathbf{A}^{\mathbf{c}}(\mathbf{x}) = [\nabla c_1(\mathbf{x}),...,\nabla c_{i+j}(\mathbf{x})]$ are the matrices of constraint gradients.

C. Convergence Analysis

From the description above, we show the proposed optimization framework of the method in Algorithm 1. Then, the convergence of the proposed algorithm will be discussed and proved in the following part.

Lemma 2: Suppose the point sequence $\{\mathbf{x}_k,\mathbf{z}_k\}$ is generated by Algorithm 1, and each point in it is the global minimum of the unconstrained subproblem $P3$, then the augmented objective function sequence is monotonically decreasing.

Proof: Note that $(\mathbf{x}_{k+1},\mathbf{z}_{k+1})$ is the global minimum point of $\varphi(\mathbf{x},\mathbf{z},\mu_{k+1})$ or $\Phi(\mathbf{x},\mathbf{z},\mu_{k+1})$, and $\mu_k \le \mu_{k+1}$, Lemma 2 can be proved. We will use $\varphi(\mathbf{x},\mathbf{z},\mu_{k+1})$ to represent the above two functions in the following part:

$$\begin{aligned} \varphi(\mathbf{x}_{k+1},\mathbf{z}_{k+1},\mu_{k+1}) = &-EE_{sys}(\mathbf{x}_{k+1}) + \frac{1}{2\mu_{k+1}}\sum_{i=1}^{NM} c_i^2(\mathbf{x}_{k+1}) \\ &+ \frac{1}{2\mu_{k+1}}\sum_{j=1}^{4NM+2N+1}[c_j'(\mathbf{x}_{k+1}) - z_{j,k+1}]^2 \\ &+ \mu_{k+1}\sum_{j=1}^{4NM+2N+1}\frac{1}{z_{j,k+1}} \\ \le &-EE_{sys}(\mathbf{x}_k) + \frac{1}{2\mu_{k+1}}\sum_{i=1}^{NM} c_i^2(\mathbf{x}_k) \end{aligned}$$

$$
\begin{aligned}
&+\frac{1}{2\mu_{k+1}}\sum_{j=1}^{4NM+2N+1}[c_j'(\mathbf{x}_k)-z_{j,k}]^2\\
&+\mu_{k+1}\sum_{j=1}^{4NM+2N+1}\frac{1}{z_{j,k}}\\
\leq&-EE_{sys}(\mathbf{x}_k)+\frac{1}{2\mu_k}\sum_{i=1}^{NM}c_i^2(\mathbf{x}_k)\\
&+\frac{1}{2\mu_k}\sum_{j=1}^{4NM+2N+1}[c_j'(\mathbf{x}_k)-z_{j,k}]^2\\
&+\mu_k\sum_{j=1}^{4NM+2N+1}\frac{1}{z_{j,k}}\\
=&\varphi\left(\mathbf{x}_k,\mathbf{z}_k,\mu_k\right). \qquad (44)
\end{aligned}
$$

Hence, Lemma 2 is proven. ■

Based on Lemma 2, the convergence for the proposed interior-point-based algorithm will be presented through Theorem 1.

Theorem 1: Suppose there is a global minimum point $(\mathbf{x}^*,\mathbf{z}^*)$, and interior-point sequence $\mathbb{D}_0 \neq \emptyset$, where $(\mathbf{x}_k,\mathbf{z}_k,\mu_k)$ denotes the point set of kth subproblem generated by Algorithm 1. Assuming $(\mathbf{x}_k,\mathbf{z}_k)$ is the global minimum point of $\varphi(\mathbf{x},\mathbf{z},\mu_k)$, then μ_k decreases monotonously, and eventually approaches 0. Therefore, any cluster point $(\bar{\mathbf{x}},\bar{\mathbf{z}})$ of $(\mathbf{x}_k,\mathbf{z}_k)$ is the global minimum of the problem $P2$.

Proof: Since there is $(\mathbf{x}_k,\mathbf{z}_k)\in\mathbb{D}_0\subset\mathbb{D}$ and $(\mathbf{x}^*,\mathbf{z}^*)$ is the local minimum point of $\varphi(\mathbf{x},\mathbf{z},\mu_k)$ on $\mathbb{D}$, that is, sequence $\varphi(\mathbf{x}_k,\mathbf{z}_k,\mu_k)$ has a lower bound. Therefore, it can be determined that the limit of $\varphi(\mathbf{x}_k,\mathbf{z}_k,\mu_k)$, that is, $\lim_{k\to\infty}\varphi(\mathbf{x}_k,\mathbf{z}_k,\mu_k)$ exists, and it can be denoted by φ^*.

Our next work is intended to prove $\varphi^*=-EE_{sys}(\mathbf{x}^*)$. Since clearly, $\varphi^*\geq -EE_{sys}(\mathbf{x}^*)$, what we need to prove is $\varphi^*\leq -EE_{sys}(\mathbf{x}^*)$. For any $\varepsilon>0$, there exists $\delta>0$, such that for any $\bar{\mathbf{x}}$ that satisfies $\|\mathbf{x}-\mathbf{x}^*\|\leq\delta$, there also exists the following relation:

$$-EE_{sys}(\bar{\mathbf{x}})-[-EE_{sys}(\mathbf{x}^*)]<\varepsilon. \qquad (45)$$

Considering μ_k monotonously decreases and approaches 0, there exists a positive k, when it is less than a specific positive number k_0. Therefore, there is:

$$\mu_k\bar{\varphi}(\bar{\mathbf{x}},\bar{\mathbf{z}})\leq\varepsilon. \qquad (46)$$

Note that $(\mathbf{x}_k,\mathbf{z}_k)$ is the global minimum of $\varphi(\mathbf{x},\mathbf{z},\mu_k)$.

$$\varphi(\mathbf{x}_k,\mathbf{z}_k,\mu_k)\leq\varphi(\bar{\mathbf{x}},\bar{\mathbf{z}},\mu_k). \qquad (47)$$

Thus, the following expression holds:

$$
\begin{aligned}
\varphi(\mathbf{x}_k,\mathbf{z}_k,\mu_k)-(-EE_{sys}(\mathbf{x}^*))&\leq\varphi(\bar{\mathbf{x}},\bar{\mathbf{z}},\mu_k)-(-EE_{sys}(\mathbf{x}^*))\\
&=\{-EE_{sys}(\bar{\mathbf{x}})-[-EE_{sys}(\mathbf{x}^*)]\}+\frac{1}{2\mu_k}\sum_{i=1}^{NM}c_i^2(\bar{\mathbf{x}})\\
&\quad+\frac{1}{2\mu_k}\sum_{j=1}^{4NM+2N+1}[c_j'(\bar{\mathbf{x}})-\bar{z}_j]^2\\
&\quad+\mu_k\sum_{j=1}^{4NM+2N+1}\frac{1}{\bar{z}_j}<\varepsilon+\varepsilon=2\varepsilon.
\end{aligned} \qquad (48)
$$

Let ε approach 0, and taking the limit of the above formula, it can be deduced that $\varphi^*\leq -EE_{sys}(\mathbf{x}^*)$. In view of $\varphi^*\geq -EE_{sys}(\mathbf{x}^*)$, we can conclude that $\varphi^*=-EE_{sys}(\mathbf{x}^*)$. Additionally, take the limit of following inequalities:

$$-EE_{sys}(\mathbf{x}^*)\leq -EE_{sys}(\mathbf{x}_k)\leq\varphi(\mathbf{x}_k,\mathbf{z}_k,\mu_k). \qquad (49)$$

We can then obtain $\lim_{k\to\infty}-EE_{sys}(\mathbf{x}_k)=-EE_{sys}(\mathbf{x}^*)$ according to the Squeeze Theorem. At this point, the proof of Theorem 1 is completed. Thus, the convergence of Algorithm 1 is easy to deduce according to Theorem 1. ■

IV. Simulation Results and Discussions

In this section, we evaluate the performance of the proposed joint optimization method on energy efficiency by comparing it to those of several benchmark schemes. The simulation results showed that the proposed method is significantly better than the benchmark methods for the above indicators. Some of the simulation parameters refer to previous works [4] and [13]. The detailed simulation parameters are provided in the next part.

A. Simulation Settings

In the simulation, the UAV flies around the curve area and provides computation assistance services for a platoon of vehicles while they are making a turn. Vehicle platoon is constructed based on the leader-follower strategy. The leader vehicle moves along a designated road at a constant velocity of 16.9 m/s, followed by other vehicles according to a particular design. The initial space headway of vehicles is predetermined as 15 m. The flight height of the UAV is fixed at H = 10 m, and it flies forth and back between the starting and ending points within the total time interval. Other parameters of G2A communication, onboard computation, and energy consumption are given in Table I.

B. Performance Comparison

In the following part, the performance of our proposed interior-point-based method, whose results are denoted as optimal values, is compared with two benchmark methods. The two benchmark methods are: i) the P-max optimization scheme, which predetermines the power as the maximum value and focuses on optimizing the time allocation, ii) the P-sto optimization scheme, which randomly generates a power value that satisfies all constraints, and then optimizes the time,

TABLE I: Simulation Parameters

Parameters	Notations	Values
Communication bandwidth	B	40 MHz
Channel power gain	g_0	-50 dB
Maximum transmission power of vehicle nodes	P_{max}	1 W
Noise power	N_0	-60 dBm
Process density	C	10^3 $cycle/bit$
Effective switched capability	λ	10^{-28}
The height of UAV	H	10 m
The number of time slots	N	100
Lane width	L	3.75 m
Turning radius	R	103.75 m
Number of vehicles	M	4
Total time interval	T	10 s
Edge computation capability	f	2 GHz

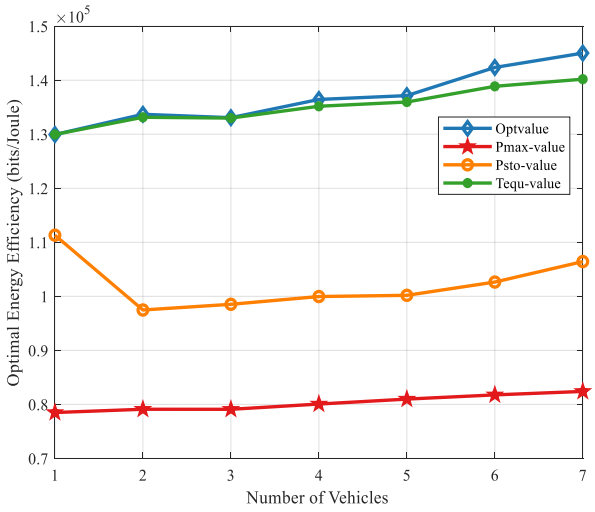

Fig. 4: The total energy efficiency under different number of platooning vehicles.

and iii) the T-equ optimization scheme, which generates an uniform time allocation scheme, then optimizes the power vector of vehicle platoon.

In order to show the advantages of our proposed method, we first compare the performance of the four schemes when the number of vehicles in vehicle formation changes. To simplify the expression, we mark our proposed method as "Optvalue", the P-max method as "Pmax-value", the P-sto method as "Psto-value", and the T-equ method as "Tequ-value". Fig. 4 shows the energy efficiency curves of the UAV-enabled MEC system under a different number of platooning vehicles, and the number of time slots is fixed to 100. As the number of vehicles increases, the energy efficiency is on an upward trend. The increase in the number of vehicles reduces the communication and time resources available to each vehicle, but also relaxes their throughput constraints (8). Because we attach a larger weight to the leading vehicle in the platoon in these experiments, the improvement of its energy efficiency increases the total weighted energy efficiency. We can also observe that with the increase of the number of platooning vehicles, the performance gap between scheme 'Opt' and scheme 'T-equ' becomes larger and larger. The main reason is that when there are few vehicles, the location distribution of vehicles is relatively close, thus the allocation of time resources is very uniform. Therefore, the time allocation scheme of the 'Opt' method is similar to the predetermined uniform scheme 'T-equ'. When the number of vehicles increases, their location distribution is more dispersed, which makes the opposite situation. Nevertheless, the proposed method achieved the best performance among the three schemes with varying vehicles. As a result, the maximum performance improvement reaches 75.99%.

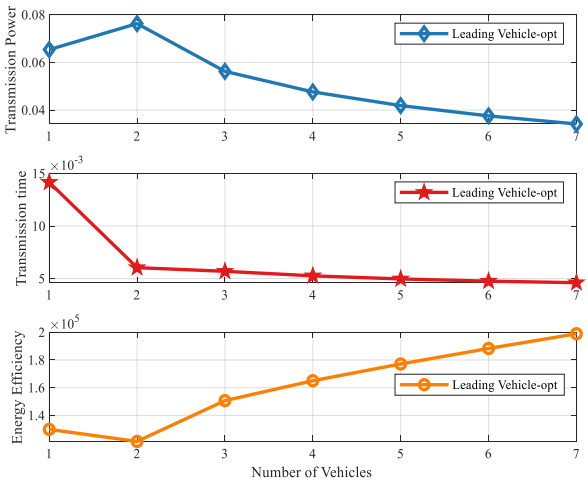

Fig. 5: Optimal communication power for leading vehicle.

Fig. 5 shows the optimal communication power, time and energy efficiency of the leading vehicle under different numbers of platooning vehicles. It can be seen that the transmission power of the leading vehicle rises first and begins to decline when the number of vehicles is more than 2, and the change of its energy efficiency (aiming at single vehicle) with the number of vehicles is just opposite to the transmission power. This is because when the number of vehicles changes from 1 to 2, the transmission time of the leading vehicle decreases sharply, so that the transmission power is increased to meet the QoS constraints (8). When the number of vehicles further increases, the decrease of transmission time is very small, while the constraints of throughput is relaxed due to the addition of other vehicles, so the transmission power decreases. For the leading vehicle, we give it a higher weight in the weight matrix. Therefore, with the increase of the number of vehicles, the system tends to improve the energy efficiency of the leading vehicle rather than following vehicles. When the number of vehicles reaches 2, its energy efficiency decreases because all the remaining weights are allocated to the single following vehicle, so that the weight of the following vehicle is temporarily higher than that of the leading vehicle. In general, it can be summarized that the construction of weight matrix has a significant impact on the system performance.

The impact of time slot numbers N on the energy efficiency is investigated, as shown in Fig. 6. In the process of changing the number of time slots, the total time interval T remains unchanged. It can be seen that the energy efficiency of the three optimization schemes all decreases as the time slots increases. The main reason is that the increase of the number

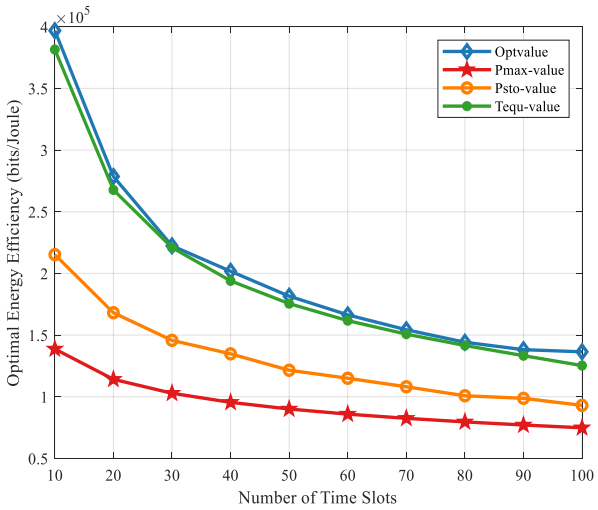

Fig. 6: The total energy efficiency under different number of time slots.

of time slots shortens the length of each time slot (the total time interval remains unchanged), thus reducing the time resources available to the vehicle platoon. In addition, the increase of time slot numbers also makes the QoS constraint (8) more stringent, resulting in a smaller feasible region and a decrease in system performance. Another fact observed is that the energy efficiency decreases more and more slowly with the further increase of the number of time slots. This is because the reduction of time length of each time slot becomes smaller and smaller with the further increase of the number of time slots. In general, in the process of the number of time slots' variation, our proposed method achieves the best performance among the four schemes, with a maximum improvement of 119.92%.

Considering the close relationship between the vehicle platoon's geometric characteristics and the allocation of computation and communication resources, we changed the shape of the vehicle platoon. In addition to the vehicle platoon, named the leader shape as shown in Fig. 7(d), there are three other shapes displayed in Figures 7(a), 7(b) and 7(c) namely geese, horizontal, and snake shapes, respectively. The first vehicle formation is the geese. The vehicles travel in a reversed "V" formation. The second vehicle platoon is a horizontal formation, where vehicles line up horizontally and run along the road. The third vehicle platoon is a longitudinal formation lined up at a specific interval along the middle road.

The impact of the vehicle platoons' shape on the system energy efficiency is evaluated as Fig. 8 shows. The above four formations have the same performance when there is one vehicle, because in this case, the vehicle's positions of the four formations are the same (The Geese shape and Leader shape have the same performance when the number of vehicles is 2, because these two shapes are also the same at this time.) And it can be seen that for three shapes of platoons: Geese, Horizontal and Leader, the change of the number of vehicles has slight impact on the system performance compared with the case of Snake shape. In our experiments, the longitudinal

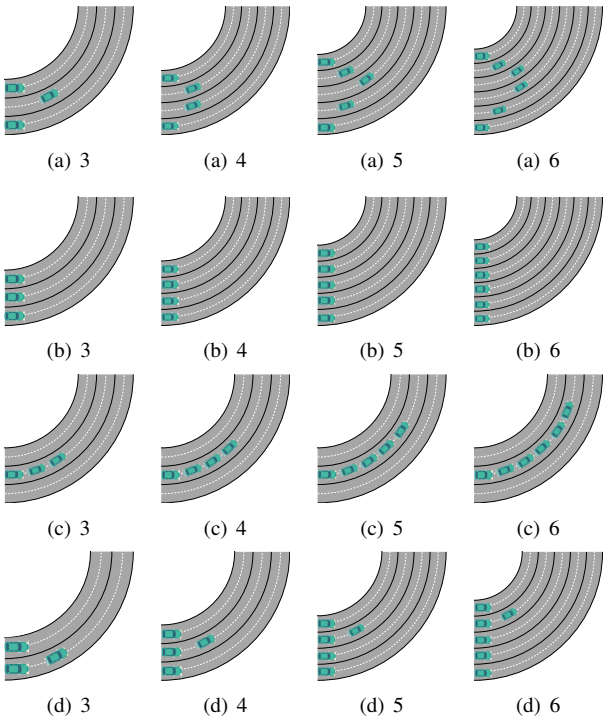

Fig. 7: Four different forms of vehicle formations (number of vehicles varies from 3 to 6). (a) geese form. (b) horizontal form. (c) snake form. (d) leader form.

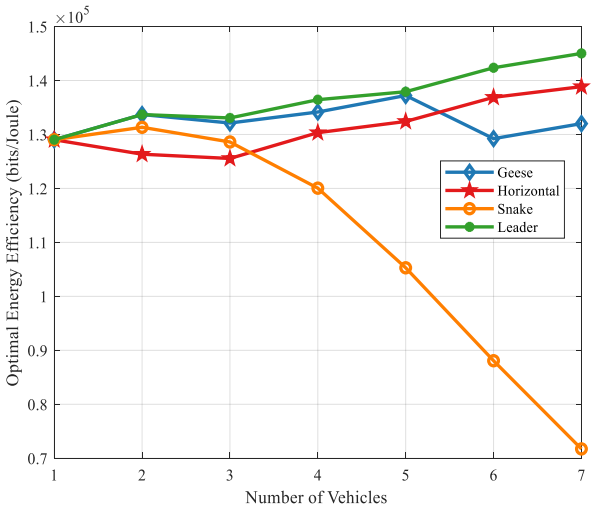

Fig. 8: The total energy efficiency under different forms of vehicle platoons.

distance of the vehicle is set to 15 m and the width of lane is set to 3.75 m. Therefore, due to its motion characteristics, the Snake shape is far more dispersed than the other three platoons. This makes the overall communication situation worse, and the communication channels of different vehicles in the platoon also vary greatly, which makes the space left for the system to schedule resources much smaller. Besides, there is little difference in the energy efficiency of the four platoon shapes above when vehicles are less than 4, with a maximum

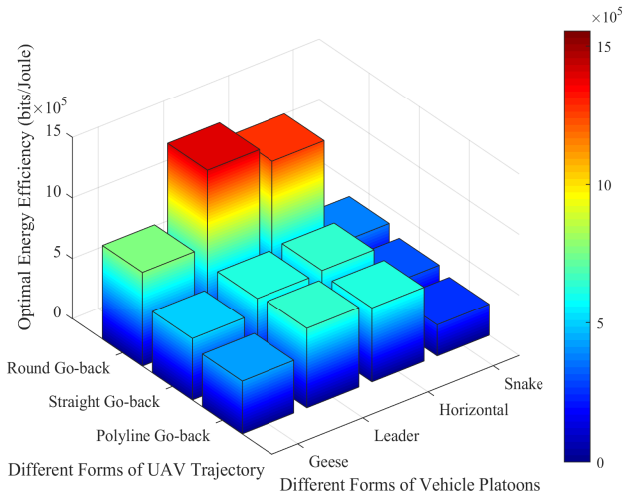

Fig. 9: Total energy efficiency under different forms of vehicle platoons and different forms of UAV trajectories.

decrease of 13.65%, which can reach 84.04% as the number of vehicles in the platoon gets bigger.

Finally, to demonstrate the effects of the UAV flights on the MEC servers' energy efficiency, we vary the UAV trajectories among the following three types: i) the polyline trajectory, the UAV first flies along the X-axis direction and then the Y-axis direction from the beginning to the end of the lane; ii) the round trajectory, the UAV travels along the arc-shaped trajectory corresponding to the path where the lead car is driving at the height H; iii) the straight round-trip trajectory, the UAV flies in a straight line from the beginning of the lane to the end. In Fig. 9, the time slots are fixed to 100, and the number of vehicles is set to 4. We illustrate the optimal energy efficiency under different forms of the UAV trajectories and vehicle platoons in Fig. 9. We can see that the system's performance under the round trajectory is better than the other two cases for all the four types of forms, while the difference of energy efficiency under the polyline trajectory and the straight trajectory is relatively small. Since the communication channel between the drone and the fleet is the best under the round trajectory due to the distance, its performance is also the most satisfactory. Another fact can be observed is that the influence of UAV trajectories also affected by the mobility characteristics of vehicle platoons. For the other two types of trajectory other than the round trajectory, the simulation results based on the configurations show that the 'Geese', the 'Horizontal', and the 'Snake' shape forms achieve better performance under the straight trajectory, while the 'Leader' shape form achieves better performance under the polyline trajectory. In Fig. 9, the energy efficiency varied from 3.01×10^5 to 1.40×10^6 (bits/Joule), and the performance difference can reach up to 281.07% due to the influence of the drone's trajectory under the same shape of vehicle platoon.

V. Conclusion

In this paper, we have developed a UAV-enabled MEC system model for turning platooning vehicles, in which communication and computation resources are scheduled to maximize the energy efficiency of MEC service. We have further considered the coupled dynamics of the two-dimensional vehicle platoon and its influence on G2A communication channel. To cope with the coupling variables and the non-convexity of the problem, we have employed a resource scheduling method based on the interior-point algorithm and the SQP algorithm, whose convergence has been discussed. Through simulation experiment, we have carried out a comparative analysis, and the results are provided to demonstrate the effectiveness and superiority of the proposed method. Our work can offer a promising approach for resource scheduling in the UAV-assisted MEC system considering coupled dynamics of two-dimensional vehicle platoon and its influence. In the future, it will be interesting to introduce reinforcement learning-based techniques into our scenario.

References

[1] Z. Du, C. Wu, T. Yoshinaga, K.-L. A. Yau, Y. Ji, and J. Li, "Federated learning for vehicular internet of things: Recent advances and open issues," *IEEE Open Journal of the Computer Society*, vol. 1, pp. 45–61, 2020.

[2] A. Eskandarian, C. Wu, and C. Sun, "Research advances and challenges of autonomous and connected ground vehicles," *IEEE Transactions on Intelligent Transportation Systems*, vol. 22, no. 2, pp. 683–711, 2021.

[3] J. Gwak, J. Jung, R. Oh, M. Park, M. A. K. Rakhimov, and J. Ahn, "A review of intelligent self-driving vehicle software research," *KSII Transactions on Internet and Information Systems (TIIS)*, vol. 13, no. 11, pp. 5299–5320, 2019.

[4] J. Zhou, D. Tian, Z. Sheng, X. Duan, and X. Shen, "Joint mobility, communication and computation optimization for uavs in air-ground cooperative networks," *IEEE Transactions on Vehicular Technology*, vol. 70, no. 3, pp. 2493–2507, 2021.

[5] W. Shi, J. Cao, Q. Zhang, Y. Li, and L. Xu, "Edge computing: Vision and challenges," *IEEE Internet of Things Journal*, vol. 3, no. 5, pp. 637–646, 2016.

[6] Y. Mao, C. You, J. Zhang, K. Huang, and K. B. Letaief, "A survey on mobile edge computing: The communication perspective," *IEEE Communications Surveys & Tutorials*, vol. 19, no. 4, pp. 2322–2358, 2017.

[7] Q. Wu, Y. Zeng, and R. Zhang, "Joint trajectory and communication design for multi-uav enabled wireless networks," *IEEE Transactions on Wireless Communications*, vol. 17, no. 3, pp. 2109–2121, 2018.

[8] Y. Liu, H.-N. Dai, Q. Wang, M. K. Shukla, and M. Imran, "Unmanned aerial vehicle for internet of everything: Opportunities and challenges," *Computer Communications*, vol. 155, pp. 66–83, 2020.

[9] Y. Zeng, R. Zhang, and T. J. Lim, "Wireless communications with unmanned aerial vehicles: Opportunities and challenges," *IEEE Communications Magazine*, vol. 54, no. 5, pp. 36–42, 2016.

[10] Z. Tan, H. Qu, J. Zhao, S. Zhou, and W. Wang, "Uav-aided edge/fog computing in smart iot community for social augmented reality," *IEEE Internet of Things Journal*, vol. 7, no. 6, pp. 4872–4884, 2020.

[11] A. Reiter, B. Prünster, and T. Zefferer, "Hybrid mobile edge computing: Unleashing the full potential of edge computing in mobile device use cases," in *2017 17th IEEE/ACM International Symposium on Cluster, Cloud and Grid Computing (CCGRID)*. IEEE, 2017, pp. 935–944.

[12] Q. Fan, J. Lin, G. Feng, Z. Gao, H. Wang, and Y. Li, "Joint service caching and computation offloading to maximize system profits in mobile edge-cloud computing," in *2020 16th International Conference on Mobility, Sensing and Networking (MSN)*. IEEE, 2020, pp. 244–251.

[13] Y. Liu, J. Zhou, D. Tian, Z. Sheng, X. Duan, G. Qu, and V. C. M. Leung, "Joint communication and computation resource scheduling of a uav-assisted mobile edge computing system for platooning vehicles," *IEEE Transactions on Intelligent Transportation Systems*, pp. 1–16, 2021.

[14] F. Zhou, Y. Wu, R. Q. Hu, and Y. Qian, "Computation rate maximization in uav-enabled wireless-powered mobile-edge computing systems," *IEEE Journal on Selected Areas in Communications*, vol. 36, no. 9, pp. 1927–1941, 2018.

[15] S. Jeong, O. Simeone, and J. Kang, "Mobile edge computing via a uav-mounted cloudlet: Optimization of bit allocation and path planning," *IEEE Transactions on Vehicular Technology*, vol. 67, no. 3, pp. 2049–2063, 2017.
[16] L. Zhang, Z.-Y. Zhang, L. Min, C. Tang, H.-Y. Zhang, Y.-H. Wang, and P. Cai, "Task offloading and trajectory control for uav-assisted mobile edge computing using deep reinforcement learning," *IEEE Access*, vol. 9, pp. 53 708–53 719, 2021.
[17] S. Zhang, J. Zhou, D. Tian, Z. Sheng, X. Duan, and V. C. Leung, "Robust cooperative communication optimization for multi-uav-aided vehicular networks," *IEEE Wireless Communications Letters*, vol. 10, no. 4, pp. 780–784, 2020.
[18] D. Yang, K. Jiang, D. Zhao, C. Yu, Z. Cao, S. Xie, Z. Xiao, X. Jiao, S. Wang, and K. Zhang, "Intelligent and connected vehicles: Current status and future perspectives," *Science China Technological Sciences*, vol. 61, no. 10, pp. 1446–1471, 2018.
[19] Y. Liu and X. Fang, "Big wave of the intelligent connected vehicles," *China Communications*, vol. 13, no. 2, pp. 27–41, 2016.
[20] H. Peng and X. Shen, "Multi-agent reinforcement learning based resource management in mec- and uav-assisted vehicular networks," *IEEE Journal on Selected Areas in Communications*, vol. 39, no. 1, pp. 131–141, 2021.
[21] J. Mei, K. Zheng, L. Zhao, L. Lei, and X. Wang, "Joint radio resource allocation and control for vehicle platooning in lte-v2v network," *IEEE Transactions on Vehicular Technology*, vol. 67, no. 12, pp. 12 218–12 230, 2018.
[22] S. Hegde, O. Blume, R. Shrivastava, and H. Bakker, "Enhanced resource scheduling for platooning in 5g v2x systems," in *2019 IEEE 2nd 5G World Forum (5GWF)*, 2019, pp. 108–113.
[23] M. Parvini, M. R. Javan, N. Mokari, B. A. Arand, and E. A. Jorswieck, "Aoi aware radio resource management of autonomous platoons via multi agent reinforcement learning," in *2021 17th International Symposium on Wireless Communication Systems (ISWCS)*, 2021, pp. 1–6.
[24] S. Hegde, L. Shi, N. J. Hernndez Marcano, R. Shrivastava, O. Blume, and R. H. Jacobsen, "Sidelink group resource scheduling for platoons in cellular vehicle-to-vehicle communications," in *2021 IEEE 93rd Vehicular Technology Conference (VTC2021-Spring)*, 2021, pp. 1–5.
[25] H. Sun, F. Zhou, and R. Q. Hu, "Joint offloading and computation energy efficiency maximization in a mobile edge computing system," *IEEE Transactions on Vehicular Technology*, vol. 68, no. 3, pp. 3052–3056, 2019.
[26] F. Zhou, H. Sun, Z. Chu, and R. Q. Hu, "Computation efficiency maximization for wireless-powered mobile edge computing," in *2018 IEEE Global Communications Conference (GLOBECOM)*, 2018, pp. 1–6.
[27] M. Li, N. Cheng, J. Gao, Y. Wang, L. Zhao, and X. Shen, "Energy-efficient uav-assisted mobile edge computing: Resource allocation and trajectory optimization," *IEEE Transactions on Vehicular Technology*, vol. 69, no. 3, pp. 3424–3438, 2020.
[28] G. Wu, Y. Miao, Y. Zhang, and A. Barnawi, "Energy efficient for uav-enabled mobile edge computing networks: Intelligent task prediction and offloading," *Computer Communications*, vol. 150, pp. 556–562, 2020.
[29] Y. Pan, X. Da, H. Hu, L. Ni, R. Xu, and H. Zhang, "Efficient design optimisation for uav-enabled mobile edge computing in cognitive radio networks," *IET Communications*, vol. 14, no. 15, pp. 2509–2515, 2020.
[30] X. Zhang, Y. Zhong, P. Liu, F. Zhou, and Y. Wang, "Resource allocation for a uav-enabled mobile-edge computing system: Computation efficiency maximization," *IEEE Access*, vol. 7, pp. 113 345–113 354, 2019.
[31] Y. Liu, K. Xiong, Q. Ni, P. Fan, and K. B. Letaief, "Uav-assisted wireless powered cooperative mobile edge computing: Joint offloading, cpu control, and trajectory optimization," *IEEE Internet of Things Journal*, vol. 7, no. 4, pp. 2777–2790, 2020.
[32] S. Bi and Y. J. Zhang, "Computation rate maximization for wireless powered mobile-edge computing with binary computation offloading," *IEEE Transactions on Wireless Communications*, vol. 17, no. 6, pp. 4177–4190, 2018.
[33] Q. Hu, Y. Cai, G. Yu, Z. Qin, M. Zhao, and G. Y. Li, "Joint offloading and trajectory design for uav-enabled mobile edge computing systems," *IEEE Internet of Things Journal*, vol. 6, no. 2, pp. 1879–1892, 2018.
[34] C. Xu, D. Li, Q. Chen, M. Liu, and K. Meng, "Joint trajectory and transmission optimization for energy efficient uav enabled elaa network," *Ad Hoc Networks*, vol. 116, pp. 102 466–102 478, 2021.
[35] Z. Wang, M. Wen, S. Dang, L. Yu, and Y. Wang, "Trajectory design and resource allocation for uav energy minimization in a rotary-wing uav-enabled wpcn," *Alexandria Engineering Journal*, vol. 60, no. 1, pp. 1787–1796, 2021.
[36] M. Werling, J. Ziegler, S. Kammel, and S. Thrun, "Optimal trajectory generation for dynamic street scenarios in a frent frame," in *2010 IEEE International Conference on Robotics and Automation*, 2010, pp. 987–993.
[37] J. Ji, K. Zhu, C. Yi, and D. Niyato, "Energy consumption minimization in uav-assisted mobile-edge computing systems: Joint resource allocation and trajectory design," *IEEE Internet of Things Journal*, vol. 8, no. 10, pp. 8570–8584, 2021.
[38] J. Gondzio, "Interior point methods 25 years later," *European Journal of Operational Research*, vol. 218, no. 3, pp. 587–601, 2012.
[39] S. Boyd, S. P. Boyd, and L. Vandenberghe, *Convex optimization*. Cambridge university press, 2004.
[40] R. H. Byrd, J. C. Gilbert, and J. Nocedal, "A trust region method based on interior point techniques for nonlinear programming," *Mathematical programming*, vol. 89, no. 1, pp. 149–185, 2000.
[41] R. H. Byrd, M. E. Hribar, and J. Nocedal, "An interior point algorithm for large-scale nonlinear programming," *Siam Journal on Optimization*, vol. 9, no. 4, pp. 877–900, 1999.

Xuting Duan received the Ph.D. degree from the School of Transportation Science and Engineering, Beihang University, Beijing, China. He is currently an assistant professor with the School of Transportation Science and Engineering, Beihang University. His current research interests are focused on connected and autonomous vehicles, vehicular ad-hoc networks, and vehicular localization.

Yukang Zhou received the B.S. degree from the School of Transportation Science and Engineering, Beihang University, Beijing, China. He is currently working towards the M.Sc. degree with the School of Transportation Science and Engineering, Beihang University. His current research interests include connected vehicles and aerial-ground cooperative networks.

Daxin Tian [M'13-SM'16] received his Ph.D. degree in computer application technology from Jilin University, Changchun, China. He is currently a University Professor with the School of Transportation Science and Engineering, Beihang University, Beijing, China. His research is focused on intelligent transportation systems, autonomous connected vehicles, swarm intelligence, and mobile computing. He was awarded the Changjiang Scholars Program (Young Scholar) of Ministry of Education of China in 2017, the National Science Fund for Distinguished Young Scholars in 2018, and the Distinguished Young Investigator of China Frontiers of Engineering in 2018. He is also a senior member of the IEEE and served as the Technical Program Committee member/Chair/Co-Chair for several international conferences including EAI 2018, ICTIS 2019, IEEE ICUS 2019, IEEE HMWC 2020, GRAPH-HOC 2020, etc.

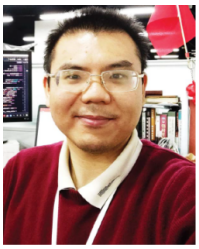

Jianshan Zhou received the B.Sc.,M.Sc., and Ph.D. degrees in traffic information engineering and control from Beihang University, Beijing, China, in 2013, 2016 and 2020, respectively. From 2017 to 2018, he was a Visiting Research Fellow with the School of Informatics and Engineering, University of Sussex, Brighton, U.K. He is currently a Postdoctoral Research Fellow supported by the Zhuoyue Program of Beihang University, and is or was the Technical Program Session Chair with the IEEE EDGE 2020 and the Youth Editorial Board Member of the Unmanned Systems Technology. He is the author or coauthor of more than 20 international scientific publications. His research interests include the modeling and optimization of vehicular communication networks and air-round cooperative networks, the analysis and control of connected autonomous vehicles, and intelligent transportation systems. He was the recipient of the First Prize in the Science and Technology Award from the China Intelligent Transportation Systems Association in 2017, the First Prize in the Innovation and Development Award from the China Association of Productivity Promotion Centers in 2020, the National Scholarships in 2017 and 2019, the Outstanding Top-Ten Ph.D. Candidate Prize from Beihang University in 2018, and the Outstanding China-SAE Doctoral Dissertation Award in 2020.

Zhengguo Sheng [SM'18] received the B.Sc. degree from the University of Electronic Science and Technology of China, Chengdu, China, in 2006, and the M.S. and Ph.D. degrees from Imperial College London, London, U.K., in 2007 and 2011, respectively. He is currently a Senior Lecturer with the University of Sussex, Brighton, U.K. Previously, he was with UBC, Vancouver, BC, Canada, as a Research Associate and with Orange Labs, Santa Monica, CA, USA, as a Senior Researcher. He has more than 100 publications. His research interests cover IoT, vehicular communications, and cloud/edge computing.

Xuemin (Sherman) Shen [M'97-M'02-'09] received the Ph.D. degree in electrical engineering from Rutgers University, New Brunswick, NJ, USA, in 1990. He is currently a University Professor with the Department of Electrical and Computer Engineering, University of Waterloo, Canada. His research focuses on network resource management, wireless network security, Internet of Things, 5G and beyond, and vehicular ad hoc and sensor networks. Dr. Shen is a registered Professional Engineer of Ontario, Canada, an Engineering Institute of Canada Fellow, a Canadian Academy of Engineering Fellow, a Royal Society of Canada Fellow, a Chinese Academy of Engineering Foreign Member, and a Distinguished Lecturer of the IEEE Vehicular Technology Society and Communications Society.

Dr. Shen received the R.A. Fessenden Award in 2019 from IEEE, Canada, Award of Merit from the Federation of Chinese Canadian Professionals (Ontario) in 2019, James Evans Avant Garde Award in 2018 from the IEEE Vehicular Technology Society, Joseph LoCicero Award in 2015 and Education Award in 2017 from the IEEE Communications Society, and Technical Recognition Award from Wireless Communications Technical Committee (2019) and AHSN Technical Committee (2013). He has also received the Excellent Graduate Supervision Award in 2006 from the University of Waterloo and the Premier's Research Excellence Award (PREA) in 2003 from the Province of Ontario, Canada. He served as the Technical Program Committee Chair/Co-Chair for IEEE Globecom'16, IEEE Infocom'14, IEEE VTC'10 Fall, IEEE Globecom'07, and the Chair for the IEEE Communications Society Technical Committee on Wireless Communications. Dr. Shen is the elected IEEE Communications Society Vice President for Technical & Educational Activities, Vice President for Publications, Member-at-Large on the Board of Governors, Chair of the Distinguished Lecturer Selection Committee, Member of IEEE ComSoc Fellow Selection Committee. He was/is the Editor-in-Chief of the IEEE IoT JOURNAL, IEEE Network, IET Communications, and Peer-to-Peer Networking and Applications.